A filamentation instability for streaming cosmic rays

Reville, B., & Bell, A. R. (2012). A filamentation instability for streaming cosmic rays. Monthly Notices of the Royal Astronomical Society, 419(3), 2433-2440. DOI: 10.1111/j.1365-2966.2011.19892.x

Published in:
Monthly Notices of the Royal Astronomical Society

Document Version:
Publisher's PDF, also known as Version of record

Monthly Notices
of the
ROYAL ASTRONOMICAL SOCIETY

Mon. Not. R. Astron. Soc. **419,** 2433–2440 (2012) doi:10.1111/j.1365-2966.2011.19892.x

A filamentation instability for streaming cosmic rays

B. Reville★ and A. R. Bell

Clarendon Laboratory, University of Oxford, Parks Road, Oxford OX1 3PU

Accepted 2011 September 26. Received 2011 September 26; in original form 2011 July 13

ABSTRACT

We demonstrate that cosmic rays form filamentary structures in the precursors of supernova remnant shocks due to their self-generated magnetic fields. The cosmic ray filamentation results in the growth of a long-wavelength instability, and naturally couples the rapid non-linear amplification on small scales to larger length-scales. Hybrid magnetohydrodynamics–particle simulations are performed to confirm the effect. The resulting large-scale magnetic field may facilitate the scattering of high-energy cosmic rays as required to accelerate protons beyond the knee in the cosmic ray spectrum at supernova remnant shocks. Filamentation far upstream of the shock may also assist in the escape of cosmic rays from the accelerator.

Key words: acceleration of particles – magnetic fields – plasmas – cosmic rays.

1 INTRODUCTION

It is generally accepted that Galactic cosmic rays are accelerated in supernova remnants. The process of diffusive shock acceleration (Axford, Leer & Skadron 1977; Krymskii 1977; Bell 1978; Blandford & Ostriker 1978) remains the most likely mechanism for producing and maintaining the observed spectrum. There is now a growing wealth of observational evidence supporting this scenario. The detection of TeV γ-ray emission from nearby remnants confirms the presence of electrons, and possibly protons, with energies of at least 10^{14} eV (e.g. Hinton & Hofmann 2009). In addition, high-resolution observations of narrow non-thermal X-ray filaments at the outer shocks of several shell-type supernova remnants favour a model in which the highest energy electrons are produced directly at the shock, consistent with the predictions of diffusive shock acceleration (e.g. Vink & Laming 2003; Bamba et al. 2005; Uchiyama et al. 2007). These filaments also provide evidence for strong magnetic field amplification in the vicinity of the shock. The generation of strong magnetic turbulence is vital for the acceleration of cosmic rays to the knee ($\sim 10^{15.5}$ eV) and above (Lagage & Cesarsky 1983; Bell & Lucek 2001).

While several mechanisms for amplifying magnetic fields to values in excess of the shock-compressed interstellar fields have been proposed, those that result in the transfer of upstream cosmic ray streaming energy to the magnetic field are of greatest relevance for diffusive shock acceleration. The non-resonant mode first identified by Bell (2004) has been demonstrated to grow rapidly; however, the characteristic wavelength of the amplified field is predominantly on a length-scale shorter than the gyroradius of the driving particles. Under certain conditions, other short-wavelength instabilities may dominate (e.g. Bret 2009; Lemoine & Pelletier 2010; Riquelme & Spitkovsky 2010; Nakar, Bret & Milosavljević 2011). While such instabilities may be sufficient to explain the large magnetic field values inferred from observations, in order to facilitate rapid acceleration to higher energies, it is necessary to generate field structure on scales comparable with the gyroradius of the highest energy particles (Bell & Lucek 2001; Reville et al. 2008).

The generation of large-scale field structures has been investigated in the context of filaments, or beams, in Bell (2005), where a pre-existing profile for the cosmic ray distribution was assumed. In this paper, we demonstrate that the distribution of relativistic particles is inherently non-uniform and that filamentation occurs as a natural consequence of cosmic ray streaming. A similar phenomenon occurs in laser plasmas whereby photon beams form filaments due to thermal self-focusing in expanding cavities (e.g. Craxton & McCrory 1984). We show here that in the case of cosmic rays, this process results in the growth of magnetic field on large scales. The development of the filamentation and large-scale field is investigated analytically in a two-dimensional (2D) slab symmetric geometry, and verified using hybrid particle–magnetohydrodynamic (MHD) simulations. The non-linear feedback between ultra-relativistic particles and the background plasma, and the resulting large-scale fields will have important implications for the acceleration of cosmic rays to energies above the knee in supernova remnants, and also their escape.

The outline of the paper is as follows. In the next section, we develop the analytic model that describes the cosmic ray filamentation. It is demonstrated that this introduces a long-wavelength instability in the precursors of supernova remnant shocks. In Section 3, we report on the numerical code used to investigate the instability, and present simulation results. The relevant time and length-scales inferred from theory and observations are addressed in Section 4. We conclude with a discussion of the implications for cosmic ray acceleration and escape of cosmic rays upstream of the shock in supernova remnants in the context of filamentation.

★E-mail: b.reville1@physics.ox.ac.uk

2 COSMIC RAY FILAMENTATION

Within the diffusion approximation of shock acceleration theory, a first-order anisotropy is introduced in the upstream particle distribution as a result of the gradient in the isotropic part of the distribution. For a shock front propagating in the positive x-direction, with velocity $u_{\rm sh}$, the resulting steady-state test-particle solution is (e.g. Drury 1983)

$$F(x, \boldsymbol{p}) = f_0(x, p)\left(1 + 3\frac{u_{\rm sh}}{c}\cos\theta\right), \tag{1}$$

where $f_0(x, p)$ is the isotropic part of the spectrum as measured in the upstream rest frame, and θ is the particle pitch angle with respect to the shock normal. It is generally understood that the current associated with the anisotropic part of the upstream particle distribution drives the growth of MHD instabilities. The resulting turbulent magnetic fields mediate the scattering that maintains the cosmic rays' quasi-isotropic distribution, ensuring a high probability that particles repeatedly cross the shock before escaping.

To investigate the behaviour in higher dimensions, it is convenient to use the Vlasov equation, which for ultra-relativistic particles can be written in the form

$$\frac{\partial f}{\partial t} + c\frac{\boldsymbol{p}}{p}\cdot\nabla f + e\left(\boldsymbol{E} + \boldsymbol{v}\times\boldsymbol{B}\right)\cdot\frac{\partial f}{\partial \boldsymbol{p}} = 0. \tag{2}$$

In a reference frame in which the upstream cosmic rays are isotropic, the distribution function $f(\boldsymbol{x}, p, t)$ is dependent only on the length of the momentum vector, not its direction, and it is straightforward to show that the magnetic field term makes no contribution. It follows that the only force relevant for calculating the particle distribution is that due to the local electric field. On average, the upstream cosmic ray distribution is isotropic in the rest frame of the shock (McClements, Dendy, Drury & Duffy 1996). Neglecting the bulk deceleration of the incoming plasma due to the cosmic ray pressure gradient, the background plasma in this frame moves towards the shock with velocity $\boldsymbol{u} = -u_{\rm sh}\hat{\boldsymbol{x}} + \delta\boldsymbol{u}$, where $\delta\boldsymbol{u}$ are the superimposed background fluid motions due to the cosmic ray current and $\hat{\boldsymbol{x}}$ is the unit vector along the direction of the shock normal. Conservation of momentum dictates that these motions are small compared to the shock velocity $|\delta\boldsymbol{u}| \ll u_{\rm sh}$, and to lowest order the local electric field is, in the ideal MHD limit, $\boldsymbol{E} = u_{\rm sh}\hat{\boldsymbol{x}}\times\boldsymbol{B}_\perp$. While this analysis is valid for all shock obliquities, we focus here on self-generated magnetic fields $B_\perp$ due to current-driven instabilities.

To investigate the role of filamentation in the plane normal to the direction of the cosmic ray streaming, we neglect the cosmic ray pressure gradient in the precursor, and restrict the analysis to the case of slab symmetry in the x-direction. Introducing the vector potential $\boldsymbol{B} = \nabla\times\boldsymbol{A}$, the local electric field is

$$\boldsymbol{E} = u_{\rm sh}\nabla A_\parallel(y, z), \tag{3}$$

where the scalar potential is $A_\parallel = \boldsymbol{A}\cdot\hat{\boldsymbol{x}}$. Inserting into equation (2), the distribution function, when observed in a reference frame in which the shock is at rest, evolves according to

$$\frac{\partial f}{\partial t} + c\frac{\boldsymbol{p}}{p}\cdot\nabla f + e\nabla(u_{\rm sh}A_\parallel)\cdot\frac{\partial f}{\partial \boldsymbol{p}} = 0, \tag{4}$$

where $u_{\rm sh}A_\parallel$ plays the role of the effective electric field potential (e.g. Krall & Trivelpiece 1973, section 8.17). On the slowly evolving MHD time-scales, the cosmic ray distribution will progress through equilibrium states

$$\frac{\partial f(\epsilon)}{\partial t} = 0, \quad \text{where } \epsilon = p - eu_{\rm sh}A_\parallel/c.$$

It follows that the phase-space distribution of the cosmic rays consists of surfaces of equal density on the momentum iso-surfaces ϵ. Hence, if $\partial f/\partial p < 0$, as is almost certainly the case, the cosmic ray number density will be locally larger (smaller) in regions of positive (negative) $A_\parallel$. Specifically, if $p \gg eu_{\rm sh}|A_\parallel|/c$, making a Taylor expansion, the number density as a function of position is

$$n_{\rm cr}(y, z) = n_0 + \frac{eu_{\rm sh}A_\parallel}{c}\int 8\pi p f_0 {\rm d}p, \tag{5}$$

where we have performed an integration by parts. Here, f_0 is the unperturbed part of the spectrum and $n_0 = \int 4\pi p^2 f_0 {\rm d}p$ is the associated uniform number density. Note that the correlation with $A_\parallel$ is dependent on the choice of orientation. If the upstream instead was chosen to lie in the half-plane $x < 0$, the density and vector potential would anti-correlate. In addition, the correlation is charge dependent, such that in the precursor, the electrons and protons will anti-correlate. Since the number density of non-thermal particles is very much less than that of the background plasma, on the length-scales of interest, charge neutrality is always maintained.

The growth of the magnetic field is driven by the resulting cosmic ray current. Transforming back to the upstream frame, from equation (5), it follows that the cosmic ray current is also a function of position

$$j_{\rm cr}(y, z) = j_0 + \chi(A_\parallel - \langle A_\parallel\rangle), \tag{6}$$

where the additional term $\langle A_\parallel\rangle$ has been added to conserve total particle number. Since lower energy particles are confined closer to the shock, the distribution is expected to fall off rapidly below a minimum momentum $p_{\rm min}$, where $p_{\rm min}(x)$ increases with distance from the shock (e.g. Eichler 1979). Assuming a power-law spectrum $f_0(p > p_{\rm min}) \propto p^{-4}$,

$$\chi = \frac{e^2u_{\rm sh}^2}{c}\int 8\pi p f_0 {\rm d}p = \frac{e^2n_0u_{\rm sh}^2}{p_{\rm min}c}.$$

It has been implicitly assumed here that the distribution function is gyrotropic such that $\boldsymbol{j}_{\rm cr}\times\hat{\boldsymbol{x}} = 0$. This naturally holds on scales larger than the cosmic ray gyroradius, but also on smaller scales provided small-angle scatterings on the background field are sufficiently frequent. All of these results have been verified using high-resolution hybrid simulations (see Section 3).

The role of a single cosmic ray filament, or beam, with fixed cosmic ray current has previously been investigated in Bell (2005). We have demonstrated here that the cosmic ray current is in fact filamentary in general. This will alter the growth of plasma instabilities, and in the next section we investigate this effect.

2.1 Filament growth

The amplification of magnetic fields in the precursors of supernova remnant shocks is a multi-scale problem. While the non-linear growth of a magnetic field, driven by cosmic ray currents, has been demonstrated via numerical simulations (e.g. Bell 2004; Ohira et al. 2009; Riquelme & Spitkovsky 2009; Stroman, Pohl & Niemiec 2009), most simulations have focused exclusively on field amplification on small scales. This is primarily due to the fact that, on larger length-scales, it becomes necessary to include the dynamics of the cosmic rays (Lucek & Bell 2000). We use the analysis of the previous section to self-consistently model the interaction between the background plasma and the cosmic rays.

Following Bell (2005), we analyse the MHD equations with an external cosmic ray current, neglecting the role of pressure gradients

and magnetic tension

$$\frac{\partial \boldsymbol{B}}{\partial t} = \nabla \times (\boldsymbol{u} \times \boldsymbol{B}), \tag{7}$$

$$\rho \frac{\mathrm{d}\boldsymbol{u}}{\mathrm{d}t} = -\boldsymbol{j}_{\mathrm{cr}} \times \boldsymbol{B}, \tag{8}$$

valid in the long-wavelength approximation. Also, from equation (7), the vector potential satisfies

$$\frac{\partial \boldsymbol{A}}{\partial t} = \boldsymbol{u} \times (\nabla \times \boldsymbol{A}). \tag{9}$$

Returning to the 2D analysis of the previous section, i.e. zero gradient in the direction of cosmic ray streaming, it follows that the parallel component of the vector potential is constant for a particular fluid element

$$\frac{\mathrm{d}A_{\parallel}}{\mathrm{d}t} = 0. \tag{10}$$

This has a number of important consequences. From equation (6), the cosmic ray current will increase in regions of large $A_{\parallel}$. Considering an idealized axisymmetric system, with maximum $A_{\parallel}$, is centred on the origin, $B_{\theta} = -\partial A_{\parallel}/\partial r > 0$, at least locally. Hence, the resulting $-\boldsymbol{j}_{\mathrm{cr}} \times \boldsymbol{B}$ force acts to push the plasma radially outwards. This spreads the region of large $A_{\parallel}$, thus focusing more cosmic rays into the filament, leading to a runaway instability. In a 2D slab symmetric geometry, this results in the spreading out of flat tabletop structures with large $A_{\parallel}$ surrounded by regions of negative $A_{\parallel}$, with large gradients in between. This is similar to the picture presented in Bell (2005, section 3), where the cosmic ray current was fixed, and the growth rate for the expansion of cavities was found to be

$$\Gamma_{\mathrm{nr}} = \left(\frac{j_{\mathrm{cr}} B_{\theta}}{r \rho_0} \right)^{1/2}, \tag{11}$$

with r the radius of the cavity and B_{θ} the magnetic field strength on that scale. Here, the focusing of the cosmic rays into the cavities will enhance the growth rate as compared with the constant current case, since j_{cr} is larger in the filaments.

For growth on small scales, the orientation of the magnetic field must be favourable. Considering a field configuration such that at early times an equal number of small-scale loops of both polarizations are randomly located within a circle of radius r_0, as shown in Fig. 1, the effect of the cosmic ray current is to expand loops of one orientation and contract the other. The net result is that the small-scale loops are predominantly of a single polarization at late times. This corresponds to a net current in the direction of the cosmic ray streaming when averaged over the area enclosed by r_0, i.e. $\langle \nabla \times \boldsymbol{B} \cdot \hat{\boldsymbol{x}} \rangle \neq 0$. As the total current enclosed by r_0 increases, the magnetic field $B_{\theta 0}$ on this scale must likewise increase. Unlike the small-scale fields, however, the growth will be independent of orientation.

To quantify the above simple picture, we combine equations (6), (7) and (8), together with the equation $\partial \boldsymbol{A}/\partial t = \boldsymbol{u} \times \boldsymbol{B}$, to give the following expression for the evolution of the filamentation:

$$\frac{\partial^2 j_{\mathrm{cr}}}{\partial t^2} = \frac{\chi B_{\perp}^2}{\rho} j_{\mathrm{cr}} + ([(\boldsymbol{u} \cdot \nabla)\boldsymbol{u}] \cdot \nabla)\, j_{\mathrm{cr}} - (\boldsymbol{u} \cdot \nabla) \frac{\partial j_{\mathrm{cr}}}{\partial t}. \tag{12}$$

The second two terms on the right-hand side of equation (12) represent the advection of $A_{\parallel}$ with the flow. On small scales, where the velocity gradients are steep, these terms dominate over the first term. However, since the continued expansion of small-scale loops is eventually inhibited by neighbouring cavities (Bell 2004; Reville et al. 2008), on sufficiently large length-scales the first term will dominate. The ordering of these terms will be verified in Section 4.

Neglecting the last two terms in equation (12), we find the following growth rate for the filamentation instability:

$$\Gamma_{\mathrm{fil}} = \sqrt{\frac{\chi B_{\perp}^2}{\rho}} = \eta \left(\frac{u_{\mathrm{sh}}}{c} \right)^2 \left(\frac{U_{\mathrm{cr}}}{\rho u_{\mathrm{sh}}^2} \right)^{1/2} \frac{e B_{\perp}^{\mathrm{rms}}}{\gamma_{\mathrm{min}} m}, \tag{13}$$

where U_{cr} is the cosmic ray energy density, $\gamma_{\mathrm{min}} = p_{\mathrm{min}}/mc$ is the Lorentz factor of the lowest energy cosmic rays driving the instability (i.e. those satisfying $p_{\mathrm{min}} c \gg e u_{\mathrm{sh}} A_{\parallel}$), and η is a numerical factor that depends on the shape of the cosmic ray spectrum. For a spectrum $f \propto p^{-4}$ in the momentum interval ($p_{\mathrm{max}} > p > p_{\mathrm{min}}$), this parameter is $\eta = 1/\sqrt{\ln(p_{\mathrm{max}}/p_{\mathrm{min}})}$. The growth rate is scale independent and depends only on the root mean square of the perpendicular magnetic field enclosed on that scale, as expected from the qualitative description above. Since the non-resonant mode discussed in Bell (2004) has a growth rate that decreases monotonically with increasing wavelength, the filamentation must dominate

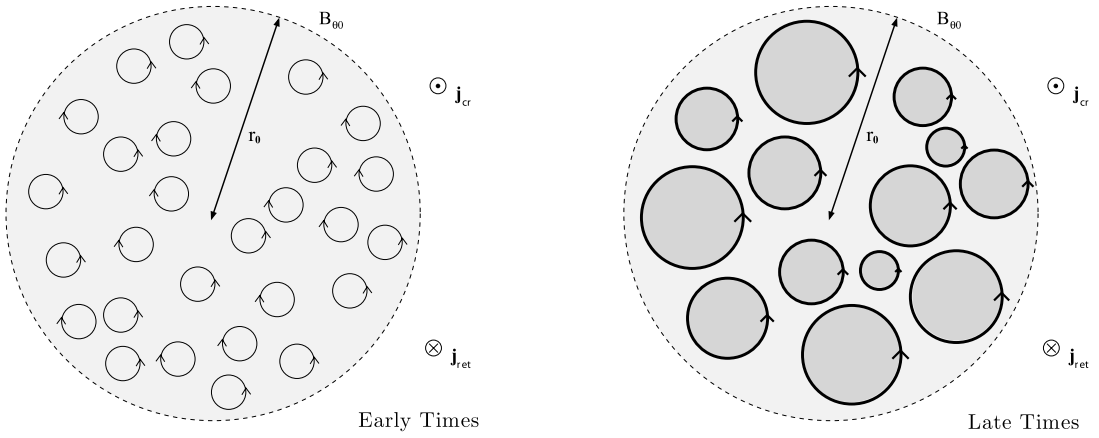

Figure 1. Illustration of the behaviour on different length-scales. $\boldsymbol{j}_{\mathrm{cr}}$ is the cosmic ray current, and $\boldsymbol{j}_{\mathrm{ret}} = (\nabla \times \boldsymbol{B})/\mu_0 - \boldsymbol{j}_{\mathrm{cr}}$ is the return current carried by the background plasma. The small-scale circles represent the expanding loops of the magnetic field of a particular handedness. At early times (left), the magnetic field contains loops of both orientations having comparable strength, and the cosmic ray current is approximately uniform. Since only loops with favourable orientation can grow, in this example counterclockwise, the cosmic rays are focused into these expanding loops, while clockwise loops contract. At later times (right), the large-scale magnetic field $B_{\theta 0}$ on scale r_0 enclosing the smaller expanding loops will have increased.

the amplification of magnetic field on some scale. However, for the growth rate of the filamentation instability to be sufficiently rapid to influence the scattering of high-energy cosmic rays, the mean squared magnetic field on small scales must be amplified to values well in excess of the ambient field. Thus, the filamentation instability can be considered as a bootstrap to the non-resonant instability described in Bell (2004, 2005). The necessary conditions for the filamentation to play an important role are discussed in detail in Section 4.

The transfer of magnetic energy from small scales to longer wavelengths in the context of diffusive shock acceleration has previously been suggested to occur via an inverse cascade (e.g. Pelletier, Lemoine & Marcowith 2006; Diamond & Malkov 2007). Whether this cascade can bridge the large separation of scales remains uncertain. The mechanism described here presents a different approach where the coupling of the scales is mediated by the filamentation. The coupling of small- and large-scale magnetic fields has also been found in simulations of sheared flows with small-scale turbulence (Yousef et al. 2008) in the context of mean-field dynamo theory. This approach has also recently been applied to the case of precursors with an external cosmic ray current (Bykov, Osipov & Ellison 2011; Schure & Bell 2011).

3 NUMERICAL SIMULATIONS

Numerical simulations are performed to verify the analysis of the previous section. To investigate these processes, it is necessary to have a kinetic description of the cosmic rays. A code has been developed similar to that described by Zachary & Cohen (1986) and Lucek & Bell (2000), where the background plasma is treated as an MHD fluid and the cosmic rays are treated using a particle-in-cell (PIC) approach. This method is appropriate for modelling plasmas in which there exists a large separation between the relevant length and time-scales associated with the thermal and non-thermal particles' kinetics. Unlike full PIC simulations, which solve Maxwell's equations directly, our simulations use the magnetic and electric fields determined from the MHD equations, i.e. the electric field is determined from ideal MHD $\boldsymbol{E} = -\boldsymbol{u} \times \boldsymbol{B}$, and the displacement current is neglected. The cosmic rays are evolved in these fields by integrating the relativistic equations of motion using the Boris method (e.g. Birdsall & Langdon 1985) and the resulting current and charge densities are deposited on the grid at each particle update using the approach of Umeda et al. (2003). Since the particles typically evolve on a shorter time-scale than the background MHD, it is necessary to integrate particle trajectories over several subcycles within each MHD update (Zachary & Cohen 1986). While this multiplies the effective number of particles in the simulation, it can also smooth out phase correlations associated with the cosmic ray current (Zachary et al. 1989; Lucek & Bell 2000). The coupled MHD–cosmic ray equations are solved using a finite-volume Godunov scheme, as described in Reville et al. (2008), with the self-consistent inclusion of temporal and spatially varying current and charge densities $j_{\rm cr}$, $Q_{\rm cr}$.

The simulations are run using a 2D slab symmetric geometry, as in the analysis of the previous section, with a periodic grid in the y–z plane, and the cosmic ray anisotropy directed out of the simulation plane in the positive x-direction. The particles are initialized as a mono-energetic distribution with a net drift velocity. Maintaining gyrotropy in the simulations and thus minimizing $j_\perp$ due to particle noise, requires that a large number of particles per cell be used. For the results shown in this paper, the particles are initialized with 1024 per cell. To minimize the noise in the particle distribution at $t = 0$, the discrete particle momentum vector in spherical coordinates, ϕ_i and μ_i, is chosen in an ordered manner, such that it satisfies the required distribution globally to a high degree of accuracy. Here, $\mu = +1$ corresponds to the positive x-direction. This is achieved by choosing the azimuthal angles with uniform spacing as $\phi_i = 2\pi M(-1)^i i/(N-1)$ for $i = 0, \ldots, N$, where N is the total number of particles and M is the number of complete rotations through 2π required. We found best results for $M = 3$. Having too many or too few revolutions in ϕ at pitch angles μ close to zero can result in a numerically introduced anisotropy in the perpendicular direction after only a relatively small number of time steps. The particle cosines μ_i are chosen between $\mu_i = -1, \ldots, 1$ with decreasing spacing $\Delta\mu_i$ such that the total distribution has a net drift with the required velocity. Finally the particles are scattered in the y–z plane using mixed radix bit-reversed fractions (Birdsall & Langdon 1985).

The 2D magnetic field is initialized by taking a sum of Fourier modes in $A_\parallel$ sampled from a user-defined spectrum, having random wave vectors $\boldsymbol{k}$ in the y–z plane (see e.g. Giacalone & Jokipii 1999). For the results shown in Fig. 2, we used a 2D Fourier spectrum $A_\parallel^2(k) \propto 1/[1 + (kL_{\rm c})^3]$, such that a perpendicular magnetic field will have a power spectrum peaking close to the length $L_{\rm c}$. Several different forms for the power spectrum have been used, and the general results are the same. The computational grid is a 512×512 square mesh with periodic boundary conditions in the y- and z-directions. The grid resolution is $\Delta x = 0.5$, where dimensionless length units are chosen such that $mc/eB_0 = 1$ with B_0 the mean magnetic field strength out of the plane. The Fourier modes were selected with uniform logarithmic spacing on the interval $4 < k/2\pi < 256$ with $L_{\rm c} = 16$, such that most of the magnetic field structure is on scales much smaller than the size of the box. The total magnetic field is then calculated by taking the curl, and projecting on to the grid using central differencing $\boldsymbol{B} = B_0\hat{\boldsymbol{x}} + \nabla \times A_\parallel \hat{\boldsymbol{x}}$. This guarantees that the field is divergence free.

The thermal background is initialized at rest with uniform density and pressure. The cosmic ray current and charge densities are also initially uniform, to within noise levels on the grid. A rather large shock velocity of $u_{\rm sh} = 0.5c$ is used to enhance the anisotropy. If the departure from isotropy is too small, a much larger number of particles are required to accurately model the perturbations to the cosmic ray current. Since the shock velocity only appears in the determination of the cosmic ray anisotropy, the use of the non-relativistic MHD equations remains valid. The numerical parameters are chosen to represent values that might be expected in a young supernova remnant: $mn_{\rm cr}/\rho_0 = 10^{-6}$ and $v_{\rm A}/c = 5 \times 10^{-4}$. The particle momentum is chosen such that the gyroradius is resolved in the simulation box, and for the results shown in Fig. 2, the particle gyroradius is $r_g = 20(B/B_0)^{-1}$. We note that with this low minimum cosmic ray energy and high shock velocity, the total cosmic ray energy density is $U_{\rm cr}/\rho_0 u_{\rm sh}^2 \approx 10^{-4}$, which is considerably smaller than what is expected in young supernova remnants. These parameters have been chosen such that the various physical processes can be easily identified in the simulations, although could also indicate that the effect should exist even in shocks that are accelerating very inefficiently. In reality, for young supernova remnants, the shock velocity would be an order of magnitude smaller and the typical cosmic ray energy several orders of magnitude larger, where $U_{\rm cr}/\rho_0 u_{\rm sh}^2$ can be as large as 30 per cent (e.g. Malkov & O'C Drury 2001). Simulations with a much higher energy density resulted in extremely rapid evacuation of zero-density cavities in the background fluid which provided insufficient time to study the growth of the magnetic field.

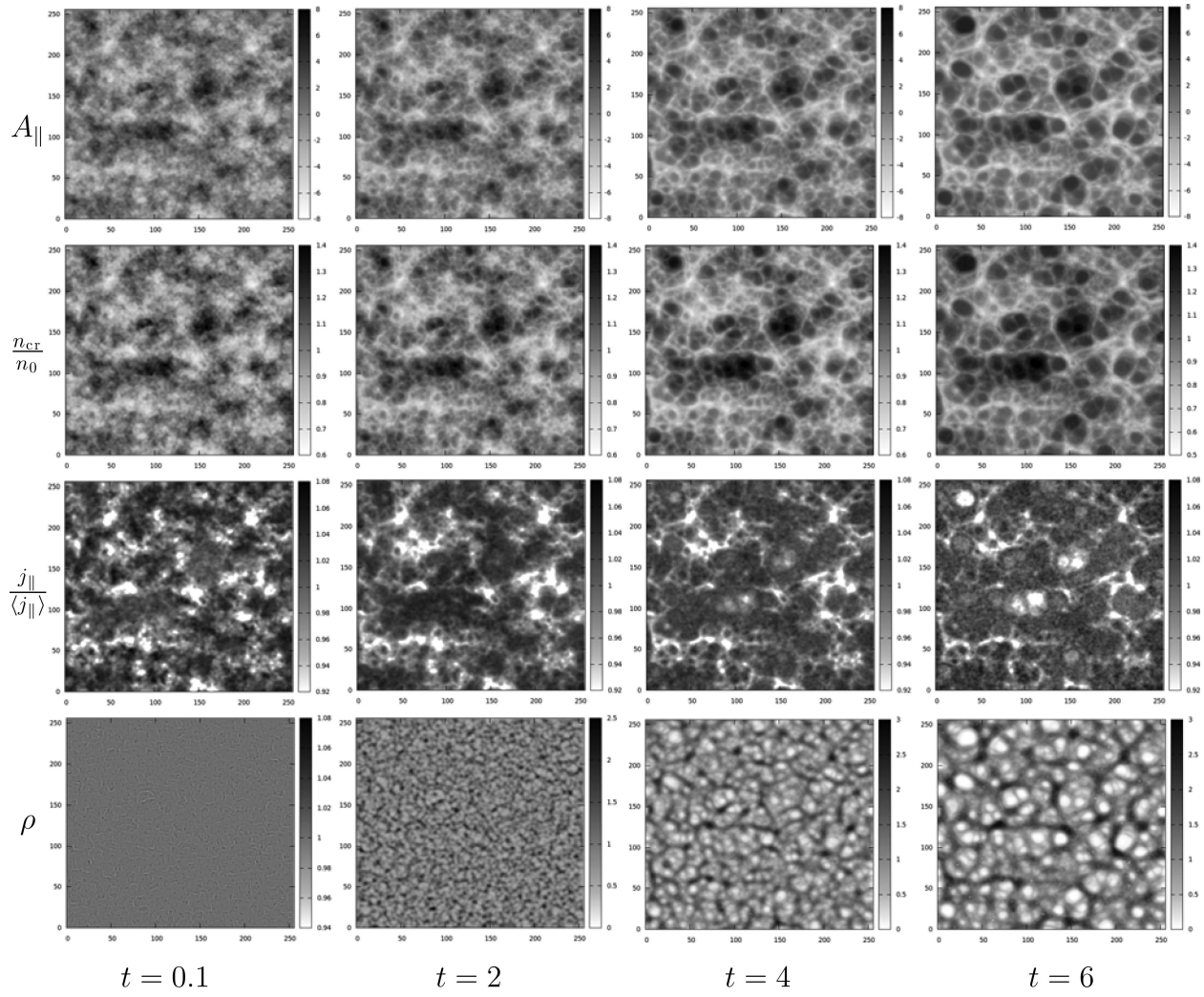

Figure 2. Time-dependent growth of the filamentation. y-z plots of $A_\parallel$, $n_{\rm cr}/n_0$, $j_\parallel/\langle j_\parallel \rangle$ and ρ at $t = 0.1, 2, 4$ and 6. Cosmic ray current is in the positive x-direction (out of the plane). Details of the simulation parameters are given in the text.

3.1 Results

The evolution of $A_\parallel$, $n_{\rm cr}$, $j_\parallel$ and ρ is shown in Fig. 2. The correlation between the vector potential and cosmic ray number density, as represented by $n_{\rm cr}$, can clearly be seen. The cosmic ray filamentation also results in the creation and expansion of low-density cavities in the thermal plasma. There also exists a correlation between the cosmic ray current $j_\parallel$ and the potential $A_\parallel$, although the features are not as sharp as with $n_{\rm cr}$. As shown in the previous section, the correlation between $A_\parallel$ and $n_{\rm cr}$ is due to fluctuations in the isotropic component f_0. The current, on the other hand, depends on higher order expansions in the anisotropy of the cosmic ray distribution and is much more difficult to capture numerically, but is clearly evident at early times. As the simulation progresses, the net streaming of cosmic rays is gradually reduced. This is always to be expected in simulations of this type (e.g. Lucek & Bell 2000), since the work done on the background plasma by the cosmic rays is $\delta W = -\boldsymbol{j}_{\rm cr} \cdot \boldsymbol{E}$, i.e. in order to extract energy from the cosmic rays, the background plasma must generate an opposing electric field. Thus, the bulk cosmic ray drift motion will be gradually decelerated, causing the correlation between $j_\parallel$ and $A_\parallel$ to become weaker as the simulation progresses. The opposing electric field will be strongest in the walls surrounding the cavities, which can account for the anti-correlations found on small scales around regions of large $A_\parallel$ at late times. The correlation on large scales is nevertheless evident even at the end of the simulation, despite a 13 per cent reduction in the net streaming velocity. In a real system, the cosmic ray streaming is continually fed by the cosmic ray pressure gradient, an effect that cannot be captured with our numerical approach.

The growth of tabletop features in the 2D plots of $A_\parallel$ is also observed. As discussed in Section 2, in two dimensions, the value of $A_\parallel$ cannot increase, but regions where $A_\parallel$ is large spread out to form the features seen in the top row of Fig. 2. It follows from equation (6) that the same must hold for the cosmic ray current. In a 3D situation, any gradients in the x-direction will act as a source term in equation (9), allowing the possibility of amplifying $A_\parallel$, resulting in continued self-focusing of the cosmic rays. This may have important implications for the upstream escape of cosmic rays from supernova remnants. We discuss this further in Section 5.

The magnetic fields at the beginning and end of the simulation are shown in Fig. 3. As found in previous simulations, regions of the strongest magnetic field are concentrated in walls surrounding the low-density cavities (Bell 2004, 2005; Reville et al. 2008). The cavities are produced by the $-\boldsymbol{j}_{\rm cr} \times \boldsymbol{B}_\perp$ force expanding low-density

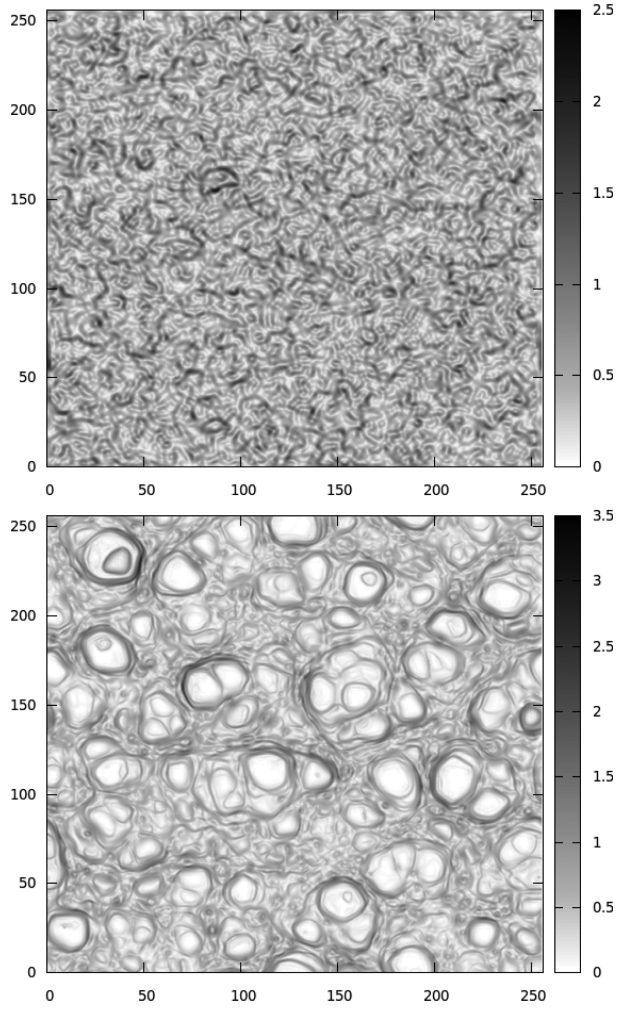

Figure 3. Plot of $|B_\perp|$ at beginning ($t = 0$) and end ($t = 8$) of the simulation. Regions of the strong magnetic field wrap around the cosmic ray filaments where the gradients in $A_\parallel$ are steep. Cavities are found to develop on a range of scales, in some cases with larger loops enclosing smaller loops.

cavities with the magnetic field frozen in to the background plasma. The largest loops appear to be on scales of $r \sim L/10$, where L is the size of the simulation box. To investigate the growth of the magnetic field on larger scales than this, we perform a Fourier analysis of the field. The evolution of the power spectrum for $B_\perp$ is shown in Fig. 4. It can be seen that structures on all wavelengths $kL/2\pi < 20$ grow monotonically with time. Since much of this structure is due to the expanding cavities, we focus on the growth of modes with $kL/2\pi < 10$, which appear to grow almost scale independently, as expected for the filamentation instability. The average measured growth rate is $\sim 0.25\Gamma_{\rm fil}$, assuming $u_{\rm sh} = 0.5c$ in equation (13). As already mentioned, in the simulations, the cosmic ray drift velocity is reduced as the simulation progresses, which may account for this reduction in comparison with the theoretically predicted growth rate, which assumed $u_{\rm sh}$ fixed. The resulting effect on the $j_\parallel$–$A_\parallel$ correlation may also contribute.

The simulations were terminated when the plasma density fell below a certain threshold. In the 3D simulations of Bell (2004), the expanding cavities can merge as field lines slide over one another, a feature that cannot be reproduced in two dimensions. Future 3D simulations will allow longer time evolution and address the issue of saturation of the large-scale magnetic field structure.

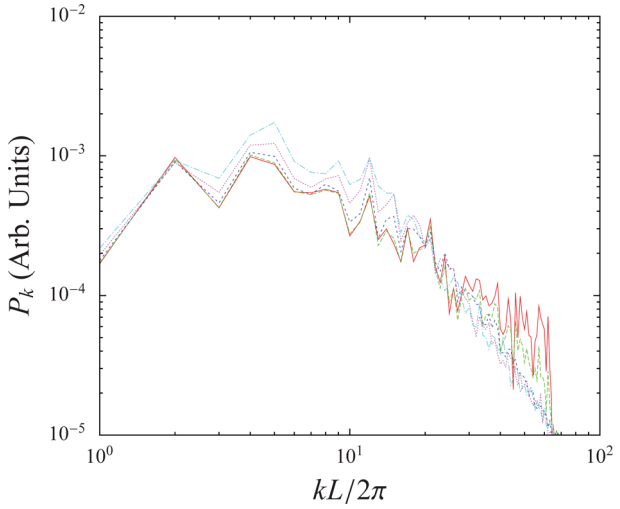

Figure 4. Fourier power spectrum of $B_\perp$ at $t = 0$, 2, 4, 6 and 8, in ascending order for $kL/2\pi < 10$, where L is the length of the sides of the simulation grid.

Finally, we emphasize that the primary difficulty in the numerical identification of the instability is choosing parameters such that the filamentation instability dominates on sufficiently small length-scales, in comparison with the size of the simulation box. Ultimately, due to the memory limitations, we are left with a relatively small dynamical range for which a Fourier analysis can be carried out, approximately one order of magnitude. In future simulations, using a different numerical technique, we hope to extend the dynamical range by at least an order of magnitude, and furthermore, to investigate the role of filamentation in three dimensions.

4 APPLICATION TO DIFFUSIVE SHOCK ACCELERATION

Observations of synchrotron X-ray emission in the vicinity of the shock suggest the presence of magnetic fields on the order of 100 μG or even larger in several supernova remnants. Recent observations have also identified the presence of a precursor in SN1006, where it is suggested that the implied field strengths are larger than the typical interstellar value (Rakowski et al. 2011), providing tentative evidence for field amplification due to the presence of cosmic rays. If these large fields are generated via cosmic ray streaming, the mechanism must account for amplification from typical seed fields $B_{\rm ISM} \sim 3$–$5\,\mu$G. Numerical simulations of cosmic ray current-driven instabilities on small scales suggest non-linear amplification of the fields to values $B_\perp^{\rm rms} \sim 30 B_{\rm ISM} \approx 100\,\mu$G (Bell 2004; Riquelme & Spitkovsky 2009). This amplification is believed to occur far upstream where only the highest energy particles interact with the interstellar medium turbulence (Zirakashvili & Ptuskin 2008; Reville, Kirk & Duffy 2009). The characteristic length-scale of the fields produced by the non-resonant instability is on too small a scale to reduce the mean-free path $\lambda_{\rm MFP}$ of the highest energy cosmic rays, as required to accelerate them beyond the Lagage–Cesarsky limit (Lagage & Cesarsky 1983). To increase the acceleration rate of the highest energy cosmic rays, the diffusion coefficient $\kappa \approx \lambda_{\rm MFP} c$ must be significantly reduced below its Bohm limit in the pre-amplified field, where the mean-free path is equal to the gyroradius $\lambda_{\rm MFP} = r_{\rm g}$. If the small-scale fields are indeed amplified to the levels inferred from observations far upstream of the shock via the non-resonant instability, as we show here, the filamentation

instability can grow on a sufficiently short time-scale to have an appreciable influence on the diffusion of the highest energy cosmic rays.

From the expression for the growth rate given in equation (13), it can be seen that the filamentation instability operates most effectively in strongly amplified small-scale turbulence, and when the cosmic rays driving the instability have lower minimum energy. However, if the energy of the cosmic rays driving the filamentation instability is too small, the particles will be trapped. This condition, as derived in Section 2 is $pc \gg eA_{\parallel}u_{\rm sh}$. Using the fiducial values from Bell (2004) (equation 21) $k_{\rm max}^{-1} \approx 2\times10^{13}$ m, the filamentation operates provided

$$E_{\rm min} \gg eA_{\parallel}u_{\rm sh} \sim ek_{\rm max}^{-1}B_{\perp}u_{\rm sh} \approx 10^{12}\left(\frac{B_{\perp}}{100\,\mu{\rm G}}\right)\left(\frac{k_{\rm max}}{2\times10^{13}\,{\rm m}}\right)^{-1}\left(\frac{u_{\rm sh}}{10^{7}\,{\rm m\,s^{-1}}}\right)\ {\rm eV}. \quad (14)$$

TeV γ-ray observations of most historical supernova remnants provide conclusive evidence for the presence of cosmic rays, either protons or electrons, that satisfy this condition.

To investigate which mechanism determines the transport properties of the highest energy cosmic rays in the precursor, we compare the growth rate of the filamentation instability to that of the streaming instability given in Bell (2004), which has a growth rate

$$\Gamma_{\rm nr} = \sqrt{\frac{j_{\rm cr}B_0k}{\rho}} \quad \text{for } k_{\rm max} > k > r_{\rm g}^{-1}. \quad (15)$$

This expression is equivalent to equation (11) on replacing B_θ/r by kB_0 (cf. Bell 2005). For $k < r_{\rm g}^{-1}$, ion-cyclotron resonance takes over and the growth rate steepens $\propto k$. Hence, the growth rate $\Gamma_{\rm nr}$ can be considered an upper limit for all k.

Since the magnetic field amplified by the non-resonant instability is on too small a scale to effectively scatter the highest energy cosmic rays driving the growth, i.e. those with $E \lesssim E_{\rm max}$, these particles will continue to gyrate about the mean field B_0. On the scale of the gyroradius of these particles $k = eB_0c/E_{\rm max}$, the ratio of the growth rate of the filamentation instability, equation (13), to the non-resonant instability is

$$\frac{\Gamma_{\rm fil}}{\Gamma_{\rm nr}} \approx \frac{B_{\perp}^{\rm rms}}{B_0}\sqrt{\frac{u_{\rm sh}}{c}\frac{E_{\rm max}}{E_{\rm min}}}, \quad (16)$$

where $E_{\rm min}$ is the corresponding energy dominating the cosmic ray current. We note here that the small-scale fields are amplified over a distance much less than the scale-height of the precursor at the outer extremity of the precursor $\approx\kappa(E_{\rm max})/u_{\rm sh}$, suggesting that $E_{\rm max}/E_{\rm min}$ should not greatly exceed unity. Thus, provided the small-scale fields can be driven to non-linear values, the filamentation instability will play a dominant role in generating the fields required to scatter the highest energy cosmic rays in supernova remnants.

The two growth rates are equal when

$$kr_{\rm g} = \frac{u_{\rm sh}}{c}\frac{\langle B_{\perp}^2\rangle}{B_0^2}, \quad (17)$$

where $r_g = E_{\rm min}/eB_0c$. This indicates, to order of magnitude, the length-scale above which the filamentation dominates over the non-resonant mode. Substitution of the parameters used in the simulations suggests that the transition occurs at $kL/2\pi \sim 10$, in agreement with what was found. In addition, comparing the terms in equation (12), it is readily seen that equation (17) corresponds to the scale on which the first term becomes comparable with the other terms.

To demonstrate the important role played by the filamentation instability, we calculate the growth rate using typical parameters for young supernova remnants. Assuming that the magnetic field is amplified initially on small length-scales to a level comparable with those inferred from observations, the typical time-scale for growth of the magnetic field on long wavelengths by the filamentation instability can be as short as

$$\Gamma_{\rm fil}^{-1} \approx 50\left(\frac{\eta}{0.2}\right)^{-1}\left(\frac{U_{\rm cr}/\rho u_{\rm sh}^2}{0.1}\right)^{-1/2}\left(\frac{u_{\rm sh}}{10^{7}\,{\rm m\,s^{-1}}}\right)^{-2} \times\left(\frac{B_{\perp}^{\rm rms}}{100\,\mu{\rm G}}\right)^{-1}\left(\frac{E_{\rm min}}{10^{14}\,{\rm eV}}\right)\ {\rm yr}. \quad (18)$$

The value of $E_{\rm min}$ driving the growth is the largest uncertainty. At the onset of the filamentation, provided the lower energy cosmic rays satisfy the condition (14), the growth can be extremely rapid. As the magnetic fields evolve, the scale of the filaments becomes comparable to the gyroradius of the lower energy particles, such that $E_{\rm min}$ should remain large. Saturation may occur when the high-energy particles become trapped on the self-generated large-scale fields. This will almost certainly affect the diffusion of cosmic rays and may even alter the transport properties of particles at different energies, which can influence the shape of the spectrum (Kirk, Duffy & Gallant 1996). Future simulations in three dimensions will help to elucidate this process further.

5 DISCUSSION

While the filamentation of photon or high-energy electron beams in laboratory laser-plasma experiments is a well-studied phenomenon (e.g. Craxton & McCrory 1984), its analogy with cosmic rays has largely been overlooked. In this paper, it has been demonstrated both analytically and confirmed with numerical simulations that the filamentation of cosmic rays is an important process that can occur in the precursors of supernova remnant shocks where diffusive shock acceleration is taking place.

In addition, we have identified a mechanism for amplifying magnetic field on large length-scales as a result of the filamentation. The process provides a natural mechanism to couple the rapid growth of the magnetic field on small scales, as driven by the non-resonant instability (Bell 2004), to length-scales comparable to, or larger than, the gyroradius of the particles driving this instability, avoiding the need for an inverse cascade. The growth time for this instability can operate on time-scales as short as a few years, provided the small-scale fields are amplified to a sufficient level. The reason for the short growth time as compared with previous calculations of linear dispersion relations is that the instability develops in non-linear small-scale magnetic fields with $\delta B^2/B_0^2 \gg 1$, unlike streaming instabilities that typically consider the growth of weak Alfvénic perturbations in the interstellar medium, where $\delta B^2/B_0^2 \ll 1$.

This has immediate implications for the maximum energy to which cosmic rays can be accelerated at supernova remnant shock fronts. The amplification of magnetic turbulence on all scales, significantly beyond the limits of quasi-linear theory, remains the most likely possibility for accelerating cosmic rays above the knee (e.g. Bell & Lucek 2001; Kirk & Dendy 2001). Using MHD simulations with a constant external cosmic ray current, Reville et al. (2008) demonstrated that the non-resonant self-generated turbulence reduced the diffusion coefficient of test particles significantly below the corresponding Bohm value in the pre-amplified field. However, due to the limited dynamic range of these simulations, the diffusion coefficient for particles with gyroradii larger than the typical

structures in the field converged to the small-angle scattering limit, where the mean-free path grows rapidly with energy $\lambda_{\rm MFP} \propto E^2$ (Reville et al. 2008; Zirakashvili & Ptuskin 2008). Thus, the generation of large-scale field structure is essential to achieve sub-Bohm diffusion at $E > 10^{15}$ eV. The filamentation instability can grow extremely rapidly once the magnetic field perturbations have been driven to non-linear levels, and may help to significantly reduce the mean-free paths of these particles. Simulations in three dimensions, with a significantly larger dynamic range, are required to confirm this.

The topic of cosmic rays escaping the source has been reinvestigated in recent years in light of developments in our understanding of the magnetic field amplification (e.g. Caprioli, Amato & Blasi 2010; Ohira, Murase & Yamazaki 2010; Drury 2011). These models typically assume a 1D or spherically symmetric model of cosmic ray diffusion. Filamentation is almost certainly important in this situation, since unlike the early 1D trapping models (e.g. Kulsrud & Zweibel 1975; Kulsrud 1979), the expansion of low-density cavities and self-focused filaments can in fact assist in the escape. This most likely occurs only far upstream, since closer to the shock, the currents in the filaments are susceptible to beam-hose-type instabilities. Again, a 3D analysis is required to investigate this further, and will be addressed in future work.

ACKNOWLEDGMENTS

The research leading to these results has received funding from the European Research Council under the European Community's Seventh Framework Programme (FP7/2007-2013)/ERC grant agreement no. 247039. BR thanks A. Spitkovsky and L. Sironi for assistance in developing the kinetic part of the numerical code, and also S. O'Sullivan, J. Kirk, K. Schure, C. Ridgers and M. Tzoufras for invaluable discussion.

REFERENCES

Axford W. I., Leer E., Skadron G., 1977, in Int. Cosmic Ray Conf. Vol. 11. p. 132
Bamba A., Yamazaki R., Yoshida T., Terasawa T., Koyama K., 2005, ApJ, 621, 793
Bell A. R., 1978, MNRAS, 182, 147
Bell A. R., 2004, MNRAS, 353, 550
Bell A. R., 2005, MNRAS, 358, 181
Bell A. R., Lucek S. G., 2001, MNRAS, 321, 433
Birdsall C. K., Langdon A. B., 1985, Plasma Physics Via Computer. McGraw-Hill, New York
Blandford R. D., Ostriker J. P., 1978, ApJ, 221, L29
Bret A., 2009, ApJ, 699, 990
Bykov A. M., Osipov S. M., Ellison D. C., 2011, MNRAS, 410, 39
Caprioli D., Amato E., Blasi P., 2010, Astropart. Phys., 33, 307
Craxton R. S., McCrory R. L., 1984, J. Appl. Phys., 56, 108
Diamond P. H., Malkov M. A., 2007, ApJ, 654, 252
Drury L. O., 1983, Rep. Prog. Phys., 46, 973
Drury L. O., 2011, MNRAS, 415, 1807
Eichler D., 1979, ApJ, 229, 419
Giacalone J., Jokipii J. R., 1999, ApJ, 520, 204
Hinton J. A., Hofmann W., 2009, ARA&A, 47, 523
Kirk J. G., Dendy R. O., 2001, J. Phys. G, 27, 1589
Kirk J. G., Duffy P., Gallant Y. A., 1996, A&A, 314, 1010
Krall N. A., Trivelpiece A. W., 1973, Principles of Plasma Physics. McGraw Hill, Tokyo
Krymskii G. F., 1977, Sov. Phys. Dokl., 22, 327
Kulsrud R. M., 1979, in Miyake S., ed., Int. Cosmic Ray Conf. Vol. 12. Int. Union of Pure & Applied Physics, p. 128
Kulsrud R., Zweibel E., 1975, in Int. Cosmic Ray Conf. Vol. 2. p. 465
Lagage P. O., Cesarsky C. J., 1983, A&A, 125, 249
Lemoine M., Pelletier G., 2010, MNRAS, 402, 321
Lucek S. G., Bell A. R., 2000, MNRAS, 314, 65
Malkov M. A., O'C Drury L., 2001, Rep. Prog. Phys., 64, 429
McClements K. G., Dendy R. O., Drury L. O., Duffy P., 1996, MNRAS, 280, 219
Nakar E., Bret A., Milosavljević M., 2011, ApJ, 738, 93
Ohira Y., Reville B., Kirk J. G., Takahara F., 2009, ApJ, 698, 445
Ohira Y., Murase K., Yamazaki R., 2010, A&A, 513, A17
Pelletier G., Lemoine M., Marcowith A., 2006, A&A, 453, 181
Rakowski C. E., Laming J. M., Hwang U., Eriksen K. A., Ghavamian P., Hughes J. P., 2011, ApJ, 735, L21
Reville B., O'Sullivan S., Duffy P., Kirk J. G., 2008, MNRAS, 386, 509
Reville B., Kirk J. G., Duffy P., 2009, ApJ, 694, 951
Riquelme M. A., Spitkovsky A., 2009, ApJ, 694, 626
Riquelme M. A., Spitkovsky A., 2010, ApJ, 717, 1054
Schure K. M., Bell A. R., 2011, MNRAS, in press (arXiv:1107.5817)
Stroman T., Pohl M., Niemiec J., 2009, ApJ, 706, 38
Uchiyama Y., Aharonian F. A., Tanaka T., Takahashi T., Maeda Y., 2007, Nat, 449, 576
Umeda T., Omura Y., Tominaga T., Matsumoto H., 2003, Comput. Phys. Commun., 156, 73
Vink J., Laming J. M., 2003, ApJ, 584, 758
Yousef T. A., Heinemann T., Schekochihin A. A., Kleeorin N., Rogachevskii I., Iskakov A. B., Cowley S. C., McWilliams J. C., 2008, Phys. Rev. Lett., 100, 184501
Zachary A. L., Cohen B. I., 1986, J. Comput. Phys., 66, 469
Zachary A. L., Cohen B. I., Max C. E., Arons J., 1989, J. Geophys. Res., 94, 2443
Zirakashvili V. N., Ptuskin V. S., 2008, ApJ, 678, 939

This paper has been typeset from a TEX/LATEX file prepared by the author.